

Chapter 9

Magnetic Resonance Imaging (MRI)

Steffen Sammet

Contents

9.1 MRI	263
9.2 Contrasts in MRI	267
9.3 Physiological and Functional MR Imaging	271
9.4 MRI Safety	275
9.5 Future MRI Applications	277
References	278

9.1 MRI

MRI is a noninvasive cross-sectional imaging modality that does not require any ionizing radiation (Sammet et al. 2010). For acquiring images, MRI uses the physical principle of magnetic resonance that was first described by Felix Bloch and Edward Purcell in 1946 who then received the Nobel Prize in Physics in 1952 for their discovery (Nature 1952). Paul Lauterbur and Peter Mansfield received a Nobel Prize in Medicine in 2003 for their description on how to acquire MR images from the human body (Lauterbur 1973; Lauterbur 2004). Since then the field of MRI has grown tremendously and is now an established and advanced imaging modality in radiology that allows to acquire high-resolution anatomical images as well as time-resolved physiological and functional datasets (Roldan-Valadez and Lopez-Mejia 2014).

S. Sammet, MD, PhD, DABR, DABMRS, FAMP (✉)
University of Chicago Medical Center, Department of Radiology, Chicago, IL, USA
e-mail: ssammet@radiology.bsd.uchicago.edu



Fig. 9.1 Clinical MRI system with the patient table in the front that can be moved inside the bore of the magnet

9.1.1 MR Imaging Principle

A patient will be moved inside the bore of a magnet with a strong static magnetic field B_0 that is in the range of 0.2 T–3 T for clinical MRI scanners (Fig. 9.1). For the typical clinical magnetic field strengths of 1.5 T and 3 T, strong superconducting magnets are required (Sammet et al. 2010).

The human body is composed of water molecules, which contain two hydrogen nuclei, or protons. The magnetic moments of these protons align with the direction of the static magnetic field inside the scanner. Oscillating electromagnetic radiofrequency fields and gradient fields are then used to acquire images from the body of the patient. The radiofrequency field B_1 is produced by an RF coil, and the fast-switching gradient fields are produced by three different coil systems (G_x , G_y , and G_z) that are embedded in the bore of the MRI scanner (Kanal et al. 1990).

9.1.1.1 Static Magnetic Field B_0

The strong static magnetic field B_0 is used to prepare chemical compounds (mainly hydrogen protons in water and fat) for imaging. The strength of the static magnetic field B_0 of an MR scanner, the magnetic flux density, is measured in the SI unit Tesla (T). Stronger static magnetic fields lead to a higher signal-to-noise ratio (SNR) and subsequently to a better image quality in the MR images or to a faster scan time. The static magnetic field of a 3 T MRI scanner is approximately 60,000 times stronger than the magnetic field of the Earth ($\sim 50 \mu\text{T}$) (Sammet et al. 2010).



Fig. 9.2 Superconducting magnet of a clinical MRI system after the removal of the covers and the patient table

These high magnetic fields cannot be achieved with permanent magnets and require superconducting magnets. A superconducting magnet is an electromagnet that is made from superconducting wires that are cooled with liquid helium (Fig. 9.2). For clinical MRI systems, these superconducting wires are most commonly made of an alloy of niobium and titanium (NbTi). The wires will be cooled below their critical temperature, the temperature at which the winding material changes from the normal resistive state to a superconducting state. The wires can conduct large electric currents in the superconducting state and have zero electrical resistance to produce strong magnet fields.

9.1.1.2 Radiofrequency Field B_1

Radiofrequency (RF) coils are designed as antennas that can transmit radiofrequency waves inside the human body and also receive the radiofrequency waves from the human body. The radiofrequency coils are built for different body parts of the patient (e.g., head coils, abdominal coils, knee coils, extremity coils) and are positioned as close as possible to the anatomical structures of interest to achieve a good image quality. A dedicated head coil is shown in Fig. 9.1 at the head end of the patient table.

The radiofrequency field B_1 causes the protons to alter their alignment relative to the static magnetic field B_0 at a higher energy state. This process is called excitation. The protons that were excited by the B_1 field will then return to their lower-energy state in a process called relaxation and will reemit RF radiation at the Larmor frequency:

$$\omega_0 = \gamma B_0 \quad (9.1)$$

Returning RF waves from the patient are picked up by the RF coils, stored in an intermediate image space (k -space), and then used to calculate an MR image with the mathematical fast Fourier transform (FFT).

9.1.1.3 Gradient Magnetic Fields G_x , G_y , and G_z

Gradient fields are used to localize the MR signal from a specific location in the human body. The three different gradient coils G_x , G_y , and G_z are embedded inside the bore of the MRI scanner and are used for slice selection (z), phase encoding (x), and frequency encoding (y) to acquire cross-sectional 2D images from any angulation or 3D datasets of the human body (Fig. 9.3). The gradient coils are responsible for the acoustic noise in an MRI scanner caused by magnetic Lorentz forces from the static magnetic field B_0 on the electric currents flowing in the gradient coils (Kanal et al. 1990).



Fig. 9.3 Gradient system of an MRI system with x -, y -, and z -gradient coils embedded in epoxy. The gradient coils are used to localize the MR signal from a specific location in the human body

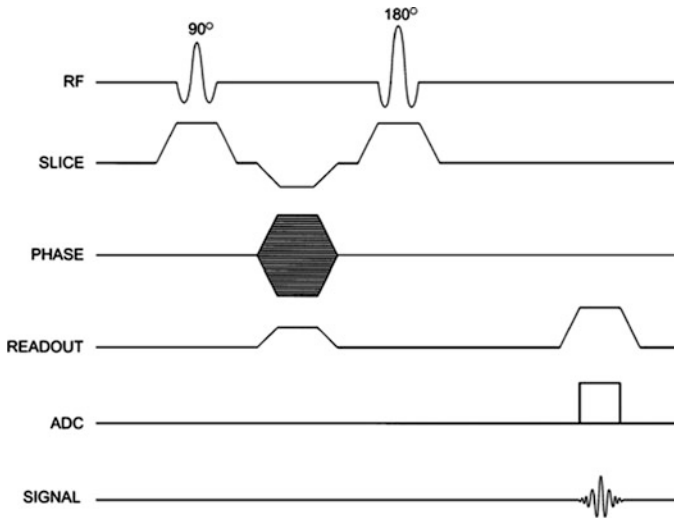


Fig. 9.4 Spin echo (SE) pulse sequence diagram with a slice selective 90° excitation pulse followed by a 180° refocusing pulses and the gradients in slice, phase, and frequency/readout direction. ADC is the time of signal acquisition and analog-to-digital signal conversion (http://bitc.bme.emory.edu/images/se_pt_1.jpg)

9.1.2 MRI Pulse Sequences

MRI pulse sequences are programs that contain the timing and duration of radiofrequency pulses and magnetic gradients to produce an image. In MRI there are two major pulse sequence groups: spin echo (SE) sequences and gradient echo (GRE) sequences. Spin echo sequences include a slice selective 90° excitation pulse followed by one or more 180° refocusing pulses (Fig. 9.4) (Mitchell et al. 1986).

Gradient echo sequences are characterized by the use of excitation pulses with flip angles of usually less than 90° , the absence of 180° RF refocusing pulses, and the use of dephasing and rephrasing gradient pulses (Fig. 9.5).

Gradient echo sequences are in general faster than spin echo sequences and allow real-time imaging of moving organs in the human body such as the heart (Li and Mirowitz 2004).

9.2 Contrasts in MRI

MRI pulse sequences are used to produce the contrast in an MRI image. In a spin echo sequence, there are generally two parameters that influence the contrast of a tissue with the spin density ρ : the repetition time (TR) and the echo time (TE):

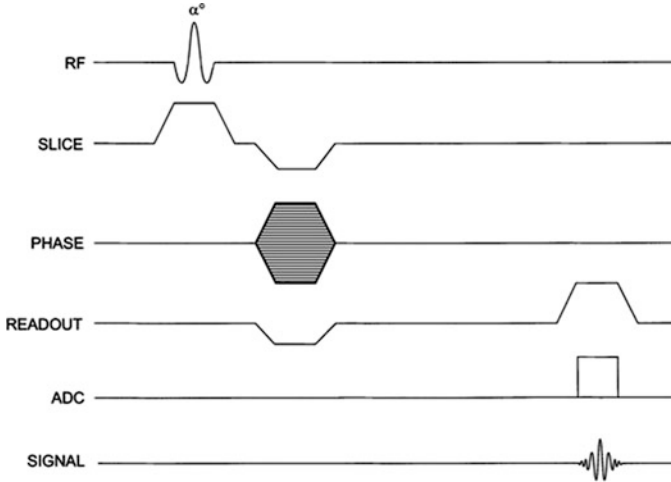


Fig. 9.5 Gradient echo (GRE) pulse sequence diagram with a slice selective excitation pulse α , which is typically smaller than 90° . The gradients in readout direction are used to produce a gradient echo when the ADC is turned on during signal acquisition (http://bitc.bme.emory.edu/images/ge_pt_1.jpg)

$$S = \rho \cdot \left(1 - e^{-\frac{TR}{T_1}}\right) \cdot e^{-\frac{TE}{T_2}}. \quad (9.2)$$

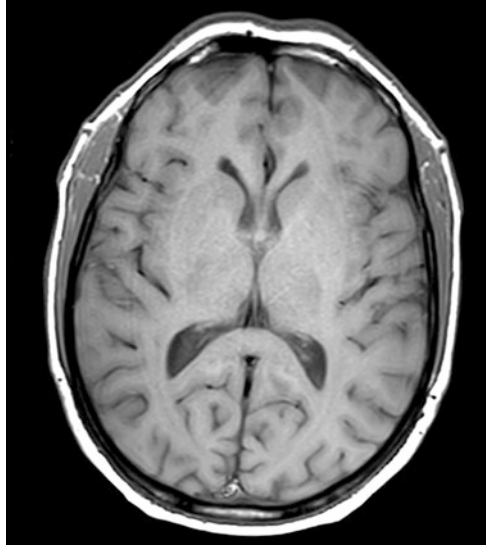
The repetition time TR is the time between two excitation pulses. The echo time (TE) is the time between an excitation pulse and MR signal sampling when the echo maximum occurs (Fig. 9.4). In a gradient echo sequence, there are in general three parameters that influence the contrast: the flip angle of the excitation pulse α , TE, and TR (Fig. 9.5) (Sammet et al. 2002).

9.2.1 T_1 Contrast

T_1 is the longitudinal or spin-lattice relaxation time. Not all energy that was put into the system with an RF pulse during the excitation returns to the RF coil. Some of the energy is lost and heats up the surrounding tissue, referred to as the lattice. The time course that describes the system's return to thermal equilibrium is mathematically described by an exponential curve. This recovery rate is characterized by the time constant T_1 (Sammet et al. 2002).

T_1 -weighted pulse sequences use short TR and short TE. Different body tissues have different T_1 relaxation times. After an excitation pulse, the longitudinal magnetization vector of fat realigns relatively quickly with the static magnetic field B_0 again, and it therefore appears bright on a T_1 -weighted image. Water

Fig. 9.6 Axial T_1 -weighted MR image of the human brain



shows much slower longitudinal magnetization realignment after a radiofrequency pulse and appears relatively dark on T_1 -weighted images (Fig. 9.6) (Sammet et al. 2002).

9.2.2 T_2 Contrast

T_2 is the transverse or spin-lattice relaxation time. Random fluctuations of the local magnetic field lead to random variations in the precession frequency of the nuclear spins in the human body. After an excitation pulse, the initial phase coherence of the nuclear spins will be lost when they get out of phase which is described by an exponential decay with the time constant T_2 . T_2 relaxation occurs more rapidly than T_1 relaxation (Sammet et al. 2002).

T_2 -weighted pulse sequences use long TR and long TE. Fluid (e.g., in the cerebrospinal fluid (CSF) spaces of the brain) appears bright on T_2 -weighted images (Fig. 9.7).

9.2.3 Proton Density Contrast

Proton density-weighted images are produced by controlling the selection of scan parameters to minimize the effects of T_1 and T_2 resulting in an image dependent primarily on the density of protons in the imaging volume. Proton density-weighted sequences use a long TR and a short TE (Fig. 9.8) (Sammet et al. 2002).

Fig. 9.7 Axial T_2 -weighted MR image of the human brain

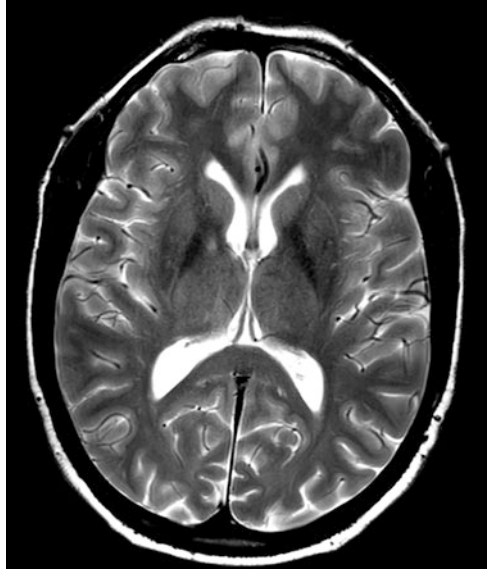
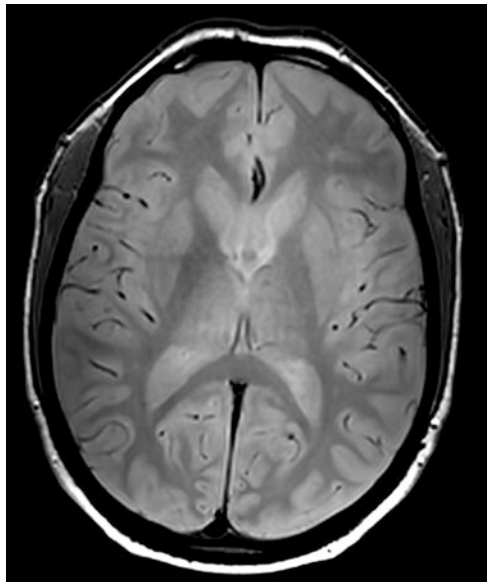


Fig. 9.8 Axial proton density-weighted MR image of the human brain



9.2.4 T_2^* Contrast

T_2^* relaxation is caused by a combination of spin-spin relaxation and magnetic field inhomogeneities. T_2^* relaxation occurs with gradient echo imaging sequences. T_2^* relaxation is faster than T_2 relaxation. In spin echo sequences, the transverse

relaxation caused by magnetic field inhomogeneities is eliminated by the 180° refocusing pulse; in gradient echo sequences, the relaxation due to magnetic field inhomogeneities cannot be eliminated. A T_2^* weighting can be achieved with a low flip angle, long echo time, and long repetition time (Yang et al. 2010).

9.3 Physiological and Functional MR Imaging

The strength of MRI is not only its great soft tissue contrast in high-resolution images but also its sensitivity to measure physiological and functional parameters in the human body. There are numerous MRI techniques and pulse sequences with different excitation pulse schemes and gradient schemes that were specifically developed to acquire anatomical physiological images from different parts of the human body (Minati et al. 2007).

9.3.1 Cardiac MRI

Cardiac MRI assesses noninvasively the function and structure of the cardiovascular system (Mousseaux et al. 1995). Gradient echo pulse sequences are important for cardiac imaging because of their speed and versatility. These gradient echo sequences are used to assess ventricular function, blood velocities, flow, valvular function, and myocardial perfusion (Wang and Amini 2012).

9.3.1.1 Cardiac Gating

There are two different gating techniques that are used in cardiac MRI: prospective gating and retrospective gating.

In prospective gating the MR data acquisition begins only after a desired physiologic signal (e.g., the R wave of the electrocardiogram (ECG)). A trigger is used to obtain MR images only at a particular time in the cardiac cycle.

In retrospective gating, the MRI data are acquired continuously, and an ECG is recorded simultaneously. The MR data can then be reordered, grouped, or correlated with phase of the cardiac cycle. Retrospective gating is typically used for cine MRI cardiac motion studies (Brinegar et al. 2008).

9.3.1.2 Cine MRI

Cine MRI produces short movies to display heart motion throughout the cardiac cycle. Cine MR images are obtained with electrocardiography (ECG) triggered segmented imaging. The segmented acquisition divides the cardiac cycle into

multiple segments (frames) to produce a series of images that can be displayed as a movie (cine) (Larson et al. 2004).

9.3.1.3 Delayed Enhancement

Delayed enhancement is performed after administration of MR contrast agents (e.g., gadolinium-based chelates). Delayed myocardial enhancement MR imaging is important to evaluate myocardial scar due to infarction. The washout of the MR contrast agent is slow in infarcted areas of the myocardium resulting in delayed enhancement after approximately 10–15 min compared to the normal myocardium (Goetti et al. 2011).

9.3.2 *Magnetic Resonance Angiography (MRA)*

Magnetic resonance angiography (MRA) techniques are used to display the vasculature and the blood flow in the human body. These sequences have clinical significance in displaying vessel occlusion and in surgical planning. MRA can be performed with an endogenous tracer (spin labeling of the flowing blood) or by injecting an exogenous contrast agent (e.g., gadolinium-based chelate) in the vasculature (Stafford Johnson et al. 1998).

There are two different MR angiography contrasts: dark blood and bright blood. Dark-blood MRA suppresses the flowing blood and displays it dark in contrary to bright-blood MRA techniques. In dark-blood MRA, the intraluminal signal is suppressed and does not generate pulsation artifacts as in the bright-blood techniques. The lack of intraluminal signal allows a better delineation of the walls of vessels or the cardiac chambers. Dark-blood techniques are used in cardiac imaging and for evaluation of atherosclerotic plaques and dissections of vessel walls (Stafford Johnson et al. 1998; Tello et al. 2003).

9.3.2.1 Time-of-Flight MRA

Time-of-flight (TOF) is a bright-blood MRA technique that uses the blood as an endogenous tracer: Fresh spins from flowing blood that enter the imaging plane produce a bright signal on time-of-flight MRA images (Heverhagen et al. 2008). Three-dimensional datasets of the vasculature can then be calculated from stacks of individual time-of-flight MRA images (maximum intensity projection) (Fig. 9.9).



Fig. 9.9 Time-of-flight (TOF) MR angiography datasets allow displaying the vessels three-dimensionally as a maximum intensity projection (MIP) by using the flowing blood as an endogenous tracer. This MIP of the human brain vasculature was generated using a magnetic field strength of 7 T

9.3.2.2 Phase-Contrast MRA

Phase-contrast angiography (PCA) is another MRI sequence that uses blood as an endogenous tracer to quantitatively assess blood flow velocities in vessels. The blood velocity is assessed by measuring the phase shift of flowing spins in the direction of magnetic field gradients. The measured phase shift is proportional to the velocity of the spins (Yamada et al. 2015).

9.3.2.3 Contrast-Enhanced MRA

In contrast-enhanced MR angiography, an exogenous contrast agent (e.g., gadolinium-based chelate) is injected into the bloodstream, while MR images are acquired. Contrast-enhanced MR angiography allows the displays of vascular structures in great detail (Ouzounian and Liu 2007).

9.3.3 Perfusion MRI

Perfusion MRI can measure parameters of tissue microvascularization, e.g., regional blood volume, mean transit time, and regional blood flow. It can be performed with an endogenous tracer (spin labeling) or an exogenous contrast agent (e.g., gadolinium-based chelate). Perfusion MRI is an important diagnostic

tool in pathological processes where perfusion changes play an important role (e.g., tumors) (Huang et al. 2014).

9.3.4 *fMRI*

Functional MRI (fMRI) uses the blood oxygenation level-dependent contrast and measures brain activity by detecting changes in blood oxygenation in brain tissue. fMRI is based on the fact that neuronal activation and cerebral blood flow changes are coupled (Detre and Floyd 2001). Deoxyhemoglobin is paramagnetic in contrary to diamagnetic oxygenated hemoglobin. Oxygenation changes of the hemoglobin molecule change the magnetic qualities of blood and subsequently the MRI signal (Janoos et al. 2010).

9.3.5 *Diffusion-Weighted MRI*

Diffusion-weighted MRI (DWI) is able to measure the random Brownian motion of water molecules within a voxel of tissue. The diffusion of water molecules parallel to geometrically aligned anatomical structures (e.g., nerve fibers) is higher than across anatomical borders of these structures (e.g., the myelin sheets of nerve fibers) (Irfanoglu et al. 2008). A DWI sequence has clinical applications in the evaluation of strokes, especially in the early phase of infarcts (Kremer et al. 2007). Conventional T₁- and T₂-weighted MR images often show an infarct only after hours in contrast to early stroke signs on DWI (Roldan-Valadez and Lopez-Mejia 2014). Diffusion-weighted MR images with two different b-values and the corresponding calculated apparent diffusion coefficient (ADC) map are shown in Fig. 9.10a, b, c.

9.3.6 *MR Spectroscopy*

Magnetic resonance spectroscopy (MRS) is an analytical technique that allows the measurement of metabolic changes in tissues. MRS gives information about biochemical processes and can complement the anatomical information of MRI. Standard MRS techniques measure the signal from hydrogen protons ¹H of different chemical compounds and display them in a frequency spectrum or even as parametric maps overlaid on anatomical images (Fig. 9.11). Multinuclear MRS techniques can also measure signals from nuclei other than ¹H, which have odd numbers of nucleons (¹³C, ²³Na, ¹⁹F, ³¹P). Current multinuclear MRS research might lead to novel clinical applications to determine metabolic changes and alterations in different diseases (Baltzer et al. 2012).

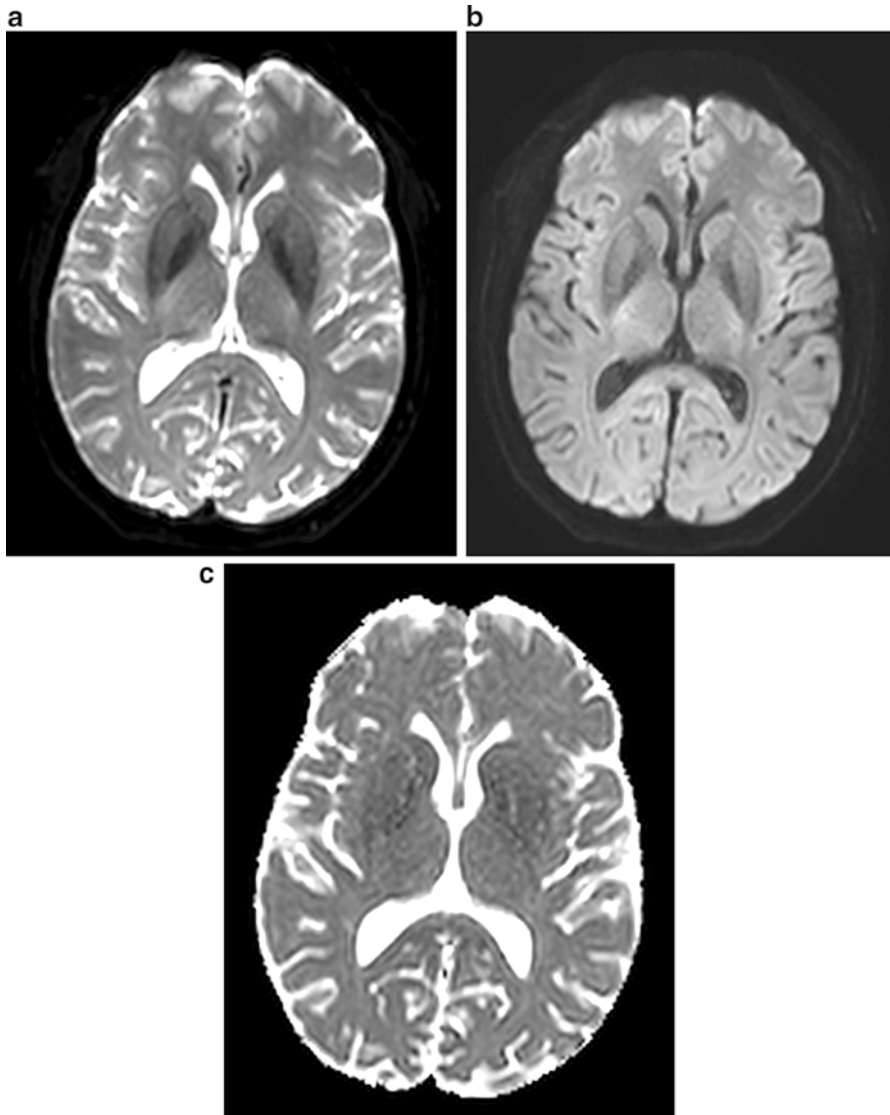


Fig. 9.10 (a) Diffusion-weighted MRI: axial DWI image of the human brain with $b = 0 \text{ s/mm}^2$, (b) with $b = 500 \text{ s/mm}^2$, and (c) corresponding calculated ADC map

9.4 MRI Safety

MRI is a very safe noninvasive imaging technique that does not require any ionizing radiation, but it is important to be aware of potential MRI safety risks for patients and personnel (Shellock and Crues 2004).

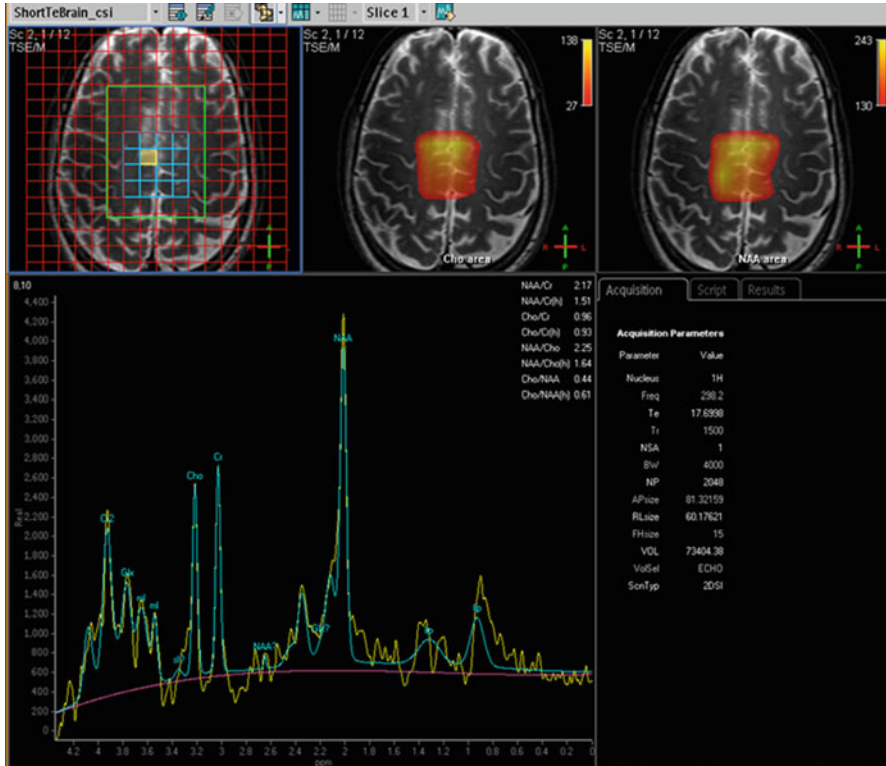


Fig. 9.11 Measurement of brain metabolites with MR spectroscopy. Chemical shift imaging at 7 T can display spectral maps and metabolic maps on top of anatomical base images

The strong static magnetic field B_0 can attract ferromagnetic objects and accelerate them in direction of the center of the bore of the MRI scanner. The static magnetic field can also influence implants and medical devices. It is therefore necessary to screen anybody before entering an MRI suite. Dedicated questionnaires are used to make sure that nobody can be injured during an MRI exam (Kanal et al. 2015).

The gradient fields G_x , G_y , and G_z are responsible for the loud noise during MRI exams and require ear protection to avoid hearing damage. Fast-switching gradient fields can also produce peripheral nerve stimulations if they exceed certain thresholds (Kanal et al. 1990).

The radiofrequency field can produce heat in body tissue. The radiofrequency exposure is limited to a maximum specific absorption rate (SAR) to avoid this heating (Kanal et al. 1990).

9.5 Future MRI Applications

9.5.1 *Ultrahigh-Field MRI*

In recent years more ultrahigh-field MRI scanners ($B_0 \geq 7$ T) became commercially available. The major benefits of ultrahigh-field MRI are an increased signal-to-noise ratio (SNR), an improved T_2^* contrast for susceptibility-weighted MRI sequences, and a greater chemical shift dispersion, which is greatly beneficial for MR spectroscopy (van der Kolk et al. 2013). The higher SNR at higher static magnetic field strengths can be used for higher spatial resolution of the MR images or a faster scan time (Speck and Tempelmann 2010).

9.5.2 *Ultrafast Sequences*

Ultrafast MR sequences allow the acquisition of an MR image in less than a second per slice. Ultrafast MR protocols use gradient echo sequences with small flip angles, very short TR, and optimized k-space filling to reduce acquisition time (Yamashita et al. 1998). The k-space trajectory determines the image contrast. Especially the fastest MRI sequence, echo planar imaging (EPI), which was first described by Mansfield in 1977 and allows the acquisition of an MR image in less than 100 ms by filling the entire k-space after one excitation, has important clinical applications in real-time cardiac imaging and in abdominal imaging to monitor contrast agent bolus arrival (Mansfield 1984).

9.5.3 *MRI-Guided Interventions*

Interventions using MRI for therapy guidance have become increasingly popular because there are many advantages of interventional MRI, including no exposure to ionizing radiation and the ability to obtain soft tissue images and to measure temperature and blood flow. MRI guidance is used, for example, for biopsies, laser therapy, high-intensity focused ultrasound (HIFU), and radiotherapy (von Schulthess and Hilfiker 1998; Da Rosa et al. 2011).

9.5.4 *Hybrid MR Imaging (MR/PET)*

Hybrid imaging is the combination of two imaging modalities into one (Pichler et al. 2008). Particularly, the combination of positron emission tomography (PET) and MRI to a whole-body MR-PET system shows the potential for various new

clinical applications to gain new insights in metabolic and functional processes in oncology as well as cardiovascular and neurologic diseases (Tudisca et al. 2015; Shah and Huang 2015).

References

- Baltzer PA, Dietzel M, Kaiser WA (2012) MR-spectroscopy at 1.5 tesla and 3 tesla. Useful? A systematic review and meta-analysis. *Eur J Radiol* 81(Suppl 1):S6–S9
- Brinegar C, Wu YJ, Foley LM, Hitchens TK, Ye Q, Ho C et al (2008) Real-time cardiac MRI without triggering, gating, or breath holding. *Conf Proc IEEE Eng Med Biol Soc* 2008:3381–3384
- Da Rosa MR, Trachtenberg J, Chopra R, Haider MA (2011) Early experience in MRI-guided therapies of prostate cancer: HIFU, laser and photodynamic treatment. *Cancer Imaging* 11 (Spec No A):S3–S8
- Detre JA, Floyd TF (2001) Functional MRI and its applications to the clinical neurosciences. *Neuroscientist* 7(1):64–79
- Goetti R, Feuchtnner G, Stolzmann P, Donati OF, Wieser M, Plass A et al (2011) Delayed enhancement imaging of myocardial viability: low-dose high-pitch CT versus MRI. *Eur Radiol* 21(10):2091–2099
- Heverhagen JT, Bourekas E, Sammet S, Knopp MV, Schmalbrock P (2008) Time-of-flight magnetic resonance angiography at 7 Tesla. *Investig Radiol* 43(8):568–573
- Huang Z, Yuh KA, Lo SS, Grecula JC, Sammet S, Sammet CL et al (2014) Validation of optimal DCE-MRI perfusion threshold to classify at-risk tumor imaging voxels in heterogeneous cervical cancer for outcome prediction. *Magn Reson Imaging* 32(10):1198–1205
- Irfanoglu MO, Machiraju R, Sammet S, Pierpaoli C, Knopp MV (2008) Automatic deformable diffusion tensor registration for fiber population analysis. *Med Image Comput Comput Assist Interv* 11(Pt 2):1014–1022
- Janoos F, Machiraju R, Sammet S, Knopp MV, Morocz IA (2010) Unsupervised learning of brain states from fMRI data. *Med Image Comput Comput Assist Interv* 13(Pt 2):201–208
- Kanal E, Shellock FG, Talagala L (1990) Safety considerations in MR imaging. *Radiology* 176 (3):593–606
- Kanal E, Froelich J, Barkovich AJ, Borgstede J, Bradley W Jr, Gimbel JR et al (2015) Standardized MR terminology and reporting of implants and devices as recommended by the American College of Radiology Subcommittee on MR Safety. *Radiology* 274(3):866–870
- Kremer S, Oppenheim C, Schmitt E, Dietemann JL (2007) Diffusion MRI: technique and clinical applications. *J Radiol* 88(3 Pt 2):428–443
- Larson AC, White RD, Laub G, McVeigh ER, Li D, Simonetti OP (2004) Self-gated cardiac cine MRI. *Magn Reson Med* 51(1):93–102
- Lauterbur PC (1973) Image formation by induced local interactions. Examples employing nuclear magnetic resonance. *Clin Orthop Relat Res* 1989(244):3–6
- Lauterbur PC (2004) Nobel lecture. All science is interdisciplinary—from magnetic moments to molecules to men. *Biosci Rep* 24(3):165–178
- Li T, Mirowitz SA (2004) Fast multi-planar gradient echo MR imaging: impact of variation in pulse sequence parameters on image quality and artifacts. *Magn Reson Imaging* 22(6):807–814
- Mansfield P (1984) Real-time echo-planar imaging by NMR. *Br Med Bull* 40(2):187–190
- Minati L, Grisoli M, Bruzzone MG (2007) MR spectroscopy, functional MRI, and diffusion-tensor imaging in the aging brain: a conceptual review. *J Geriatr Psychiatry Neurol* 20(1):3–21
- Mitchell MR, Tarr RW, Conturo TE, Partain CL, James AE Jr (1986) Spin echo technique selection: basic principles for choosing MRI pulse sequence timing intervals. *Radiographics* 6(2):245–260

- Mousseaux E, Sapoval M, Gaux JC (1995) MRI in cardiology: clinical applications and perspectives. *Ann Radiol (Paris)* 38(1–2):55–68
- Nature (1952) Nobel prize for physics, 1952. *Nature* 170(4335):911–912
- Ouzounian M, Liu PP (2007) Review: contrast-enhanced MRA is more sensitive and specific than CT angiography or ultrasonography for detection of lower-limb PAD. *ACP J Club* 147(3):77
- Pichler BJ, Judenhofer MS, Wehrl HF (2008) PET/MRI hybrid imaging: devices and initial results. *Eur Radiol* 18(6):1077–1086
- Roldan-Valadez E, Lopez-Mejia M (2014) Current concepts on magnetic resonance imaging (MRI) perfusion-diffusion assessment in acute ischaemic stroke: a review & an update for the clinicians. *Indian J Med Res* 140(6):717–728
- Sammet S, Bock M, Streckenbach M, Bachert P (2002) Proton spinlocking and T1 rho-weighted MR imaging at 1.5 T. *Z Med Phys* 12(1):16–23
- Sammet S, Koch RM, Aguila F, Knopp MV (2010) Residual magnetism in an MRI suite after field-rampdown: what are the issues and experiences? *J Magn Reson Imaging* 31(5):1272–1276
- Shah SN, Huang SS (2015) Hybrid PET/MR imaging: physics and technical considerations. *Abdom Imaging* 40(6):1358–1365
- Shellock FG, Crues JV (2004) MR procedures: biologic effects, safety, and patient care. *Radiology* 232(3):635–652
- Speck O, Tempelmann C (2010) Human 7T MRI: first clinical and neuroscientific applications. *Neuroradiol J* 23(5):535–546
- Stafford Johnson DB, Prince MR, Chenevert TL (1998) Magnetic resonance angiography: a review. *Acad Radiol* 5(4):289–305
- Tello R, Mitchell PJ, Witte DJ, Thomson KR (2003) T2 dark blood MRA for renal artery stenosis detection: preliminary observations. *Comput Med Imaging Graph* 27(1):11–16
- Tudisca C, Nasoodi A, Fraioli F (2015) PET-MRI: clinical application of the new hybrid technology. *Nucl Med Commun* 36(7):666–678
- van der Kolk AG, Hendrikse J, Zwanenburg JJ, Visser F, Luijten PR (2013) Clinical applications of 7 T MRI in the brain. *Eur J Radiol* 82(5):708–718
- von Schulthess GK, Hilfiker P (1998) Interventional MRI: the way to the future. *J Invasive Cardiol* 10(9):571–577
- Wang H, Amini AA (2012) Cardiac motion and deformation recovery from MRI: a review. *IEEE Trans Med Imaging* 31(2):487–503
- Yamada S, Tsuchiya K, Bradley WG, Law M, Winkler ML, Borzage MT et al (2015) Current and emerging MR imaging techniques for the diagnosis and management of CSF flow disorders: a review of phase-contrast and time-spatial labeling inversion pulse. *AJNR Am J Neuroradiol* 36(4):623–630
- Yamashita Y, Tang Y, Takahashi M (1998) Ultrafast MR imaging of the abdomen: echo planar imaging and diffusion-weighted imaging. *J Magn Reson Imaging* 8(2):367–374
- Yang X, Sammet S, Schmalbrock P, Knopp MV (2010) Postprocessing correction for distortions in T2* decay caused by quadratic cross-slice B0 inhomogeneity. *Magn Reson Med* 63(5):1258–1268